Journal of Medicinal Chemistry

Article

Cite This: J. Med. Chem. 2019, 62, 8996−9007

pubs.acs.org/jmc

Discovery of a Potent and Selective Fragment-like Inhibitor of Methyllysine Reader Protein Spindlin 1 (SPIN1)

Yan Xiong,[†,§§] Holger Greschik,[‡,§§] Catrine Johansson,[§,§§] Ludwig Seifert,[∥] Johannes Bacher,[∥] Kwang-su Park,[†] Nicolas Babault,[†] Michael Martini,[†] Vincent Fagan,[⊥] Fengling Li,[#] Irene Chau,[#] Thomas Christott,[⊥] David Dilworth,[#] Dalia Barsyte-Lovejoy,[#,¶] Masoud Vedadi,[#,▽] Cheryl H. Arrowsmith,[#,○] Paul Brennan,[⊥] Oleg Fedorov,[⊥] Manfred Jung,[∥,††,‡‡] Gillian Farnie,[⊥] Jing Liu,[†] Udo Oppermann,[*,§] Roland Schüle,[*,‡,♦,‡‡] and Jian Jin[*,†]

[†]Mount Sinai Center for Therapeutics Discovery, Departments of Pharmacological Sciences and Oncological Sciences, Tisch Cancer Institute, Icahn School of Medicine at Mount Sinai, New York, New York 10029, United States

[‡]Department of Urology and Center for Clinical Research, University Freiburg Medical Center, Freiburg 79106, Germany

[§]Structural Genomics Consortium, Botnar Research Center, NIHR Oxford BRU, University of Oxford, Oxford OX37LD, U.K.

[∥]Institute of Pharmaceutical Sciences, University of Freiburg, Freiburg 79104, Germany

[⊥]Structural Genomics Consortium & Target Discovery Institute, University of Oxford, Oxford OX37DQ and OX37FZ, U.K.

[#]Structural Genomics Consortium and [○]Princess Margaret Cancer Centre and Department of Medical Biophysics, University of Toronto, Toronto, Ontario M5G 1L7, Canada

[¶]Nature Research Center, Akademijos 2, Vilnius 08412, Lithuania

[▽]Department of Pharmacology and Toxicology, University of Toronto, Toronto, Ontario M5S 1A8, Canada

[♦]BIOSS Centre of Biological Signalling Studies, University of Freiburg, Freiburg 79106, Germany

[††]German Cancer Research Centre (DKFZ), Heidelberg 69120, Germany

[‡‡]German Cancer Consortium (DKTK), Freiburg 79106, Germany

Supporting Information

ABSTRACT: By screening an epigenetic compound library, we identified that UNC0638, a highly potent inhibitor of the histone methyltransferases G9a and GLP, was a weak inhibitor of SPIN1 (spindlin 1), a methyllysine reader protein. Our optimization of this weak hit resulted in the discovery of a potent, selective, and cell-active SPIN1 inhibitor, compound **3** (MS31). Compound **3** potently inhibited binding of trimethyllysine-containing peptides to SPIN1, displayed high binding affinity, was highly selective for SPIN1 over other epigenetic readers and writers, directly engaged SPIN1 in cells, and was not toxic to nontumorigenic cells. The crystal structure of the SPIN1−compound **3** complex indicated that it selectively binds tudor domain II of SPIN1. We also designed a structurally similar but inactive compound **4** (MS31N) as a negative control. Our results have demonstrated for the first time that potent, selective, and cell-active fragment-like inhibitors can be generated by targeting a single tudor domain.

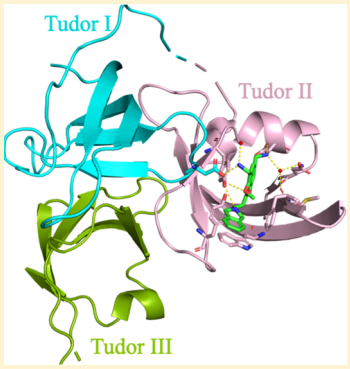

INTRODUCTION

Epigenetic regulation plays an important role in gene expression and transcription, which are critical for a variety of cellular processes. Epigenetic modifications can be divided into two main categories: DNA methylation and histone modifications.[1] Histone post-translational modifications (PTMs)[2] require three types of proteins: the enzymes that create the modifications (the "writers"),[3−7] the enzymes that remove the modifications (the "erasers"),[7,8] and the proteins that recognize the modifications (the "readers").[9,10] Growing evidence suggests that reader proteins are implicated in a number of human diseases including cancer.[11] Therefore, reader proteins are increasingly being pursued as potential therapeutic targets.[12,13] However, unlike the significant progress made in the discovery of small-molecule inhibitors of histone methyltransferases (MTs), bromodomain-containing proteins (which recognize acetylated lysine residues), and histone demethylases,[5−7,14−16] only a very limited number of small-molecule inhibitors targeting methyllysine reader proteins have been reported, including UNC1215 (a potent and selective L3MBTL3 inhibitor), UNC3866 (a potent and selective peptide-based CBX7/4 inhibitor), EML631 (a selective and cell-active SPIN1 inhibitor with 685 Da molecule

Received: March 25, 2019
Published: July 1, 2019

DOI: 10.1021/acs.jmedchem.9b00522
J. Med. Chem. 2019, 62, 8996−9007

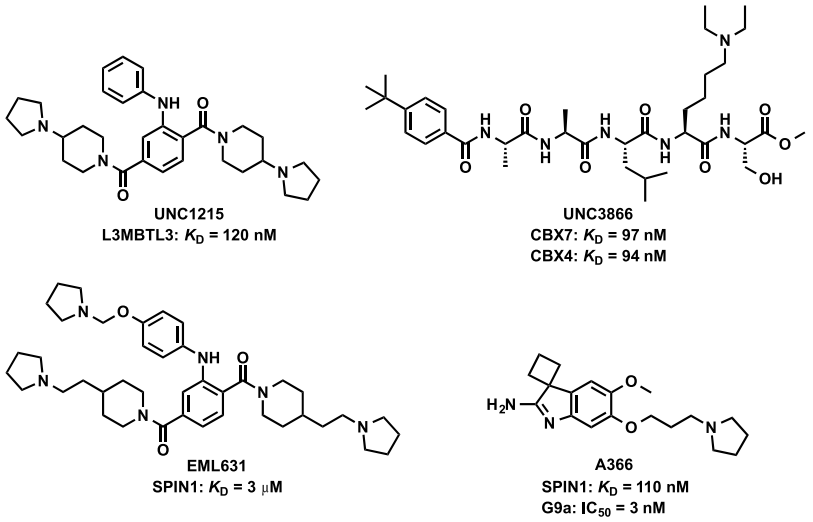

Figure 1. Representative inhibitors of methyllysine reader proteins.

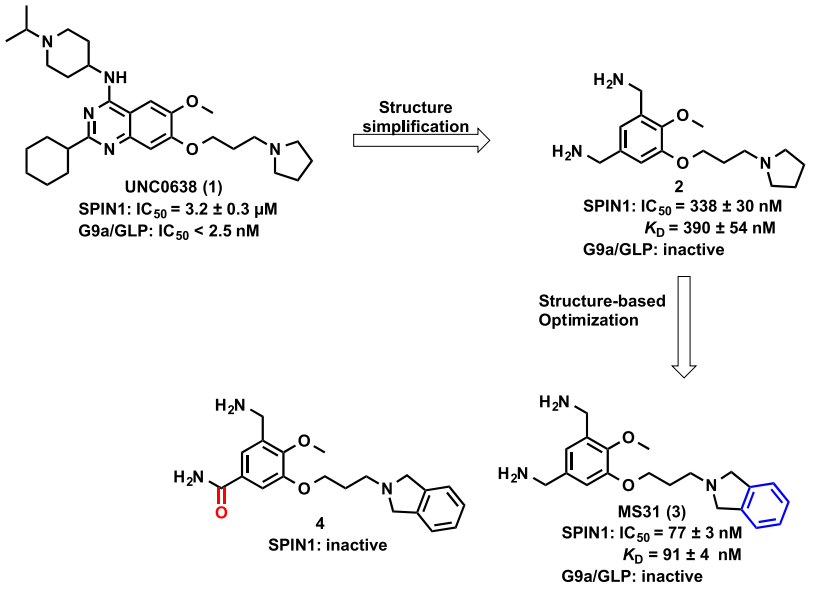

Figure 2. Discovery of compound **3** and its inactive control compound **4**.

weight), and A366 (a nonselective SPIN1 inhibitor) (Figure 1).[17−24] Furthermore, it is quite challenging to achieve sufficient potency and selectivity by targeting a single methyllysine reader domain such as a tudor domain or malignant brain tumor (MBT) domain as several reported potents, and selective inhibitors of methyllysine reader proteins such as UNC1215 and EML631 achieved their potency and selectivity by simultaneously targeting two methyllysine reader domains.[21,24]

SPIN1 (spindlin 1) is a chromatin reader protein, which recognizes trimethylated histone H3 lysine 4 (H3K4me3) through the protein−protein interaction at the defined "aromatic cage" in tudor domain II, and the interaction between asymmetrically dimethylated histone H3 arginine 8 (H3R8me2a) and tudor domain I further increases the affinity.[25−27] SPIN1 was found to be overexpressed in several types of malignant tumors, including ovarian cancer, certain types of liver carcinomas, nonsmall-cell lung cancers, and liposarcoma.[28−33] Upregulation of SPIN1 has been shown to increase cellular proliferation, abnormal mitosis, and chromosomal instability.[34] In addition, SPIN1 is involved in several signaling pathways, such as Wnt/TCF-4 and RET signaling pathways.[29,35] Therefore, small molecules that selectively disrupt the protein−protein interactions between SPIN1 and its respective binding partners (such as H3K4me3) are valuable chemical tools for investigating biological functions of SPIN1 and assessing the potential of SPIN1 as a therapeutic target. Two small-molecule inhibitors of SPIN1 have been reported to date. We previously reported that A366 (Figure 1) was a potent but not a selective inhibitor of SPIN1 (Figure S1).[23] A class of bivalent compounds represented by EML631 (Figure 1) that occupy tudor domains I and II of SPIN1 were shown to be selective and cell-active inhibitors of SPIN1 with a relatively weak binding affinity.[24] The relatively high molecule weight of EML631 (685 Da) may also render difficulties for further optimization.

Fragment-like inhibitors may possess high intrinsic binding energy and often exhibit high ligand efficiency (LE).[36,37] Their low molecular weights leave large room for installing additional functional groups in lead optimization, which could result in

DOI: 10.1021/acs.jmedchem.9b00522
J. Med. Chem. 2019, 62, 8996−9007

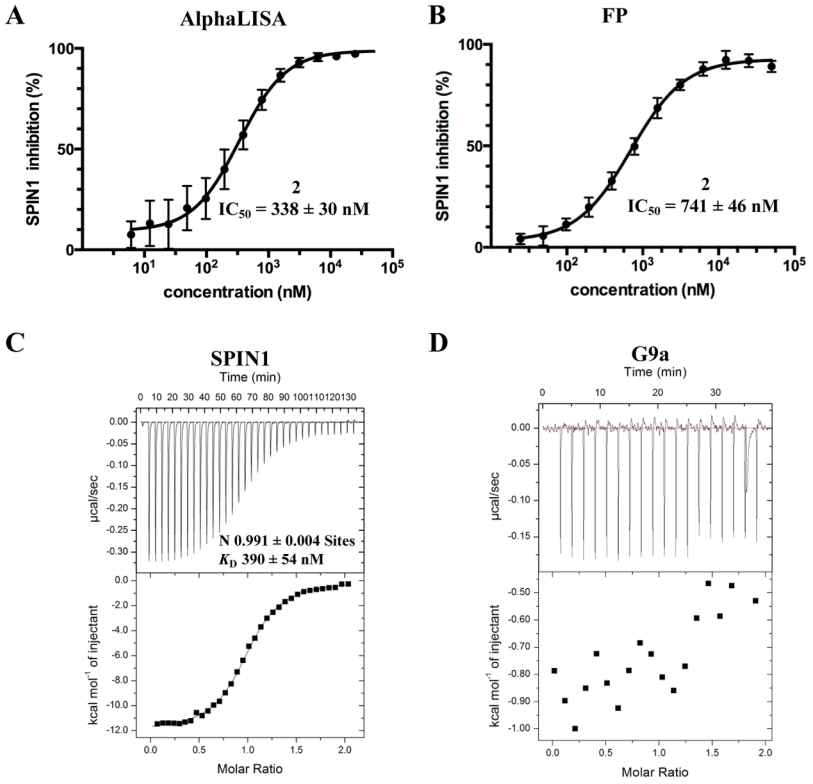

Figure 3. Compound **2** is a selective SPIN 1 inhibitor. Compound **2** inhibited the interactions between SPIN1 and H3K4me3 in a concentration dependent manner with IC_{50} values of (A) 338 ± 30 nM in AlphaLISA assay (n = 3) and (B) 741 ± 46 nM in FP assay (n = 3). (C) Compound **2** bound SPIN1 with a K_D value of 390 ± 54 nM in ITC assay (n = 3). (D) Compound **2** did not bind G9a.

drug candidates with higher potency and improved physicochemical properties, such as aqueous solubility, membrane permeability, and oral bioavailability. Therefore, fragment-like inhibitors are valuable starting points for drug development efforts, in addition to being useful tools for chemical biology studies.[38] Here, we report our discovery of a fragment-like inhibitor, compound **3** (MS31) with a molecular weight less than 350, which potently and selectively disrupted the protein−protein interactions between SPIN1 and H3K4me3.

RESULTS AND DISCUSSION

Discovery of a Fragment-like Hit (Compound 2). Using AlphaLISA and fluorescence polarization (FP)-based biochemical assays, we screened the epigenetic compound library generated by our lab, which includes hundreds of small-molecule modulators of epigenetic writers, readers, and erasers, and identified UNC0638 (compound **1**, Figure 2), a highly potent inhibitor of the histone MTs G9a and GLP,[39,40] as a weak SPIN1 inhibitor (IC_{50} = 3.2 ± 0.3 μM (AlphaLISA) and 7.4 ± 0.4 μM (FP)) (Figure S1). To improve potency and selectivity of UNC0638 for SPIN1 over G9a and GLP, we analyzed the cocrystal structure of compound **1** in the complex with G9a (PDB: 3RJW)[41] and the cocrystal structure of SPIN1 in the complex with a H3 peptide (PDB: 4H75)[26] and generated a docking model of compound **1** in the complex with SPIN1 (Figure S2). The docking model suggests that the 3-(pyrrolidin-1-yl)propoxyl group of compound **1** likely mimics H3K4me3, interacting with the aromatic cage of the SPIN1 tudor domain II, while the 4-amino piperidine group on the quinazoline ring extends out of the SPIN1 tudor domain II and the 2-cyclohexyl group on the quinazoline ring does not appear to make any interactions. Based on these observations, we simplified the structure of compound **1** by replacing the 2,4-disubstituted quinazoline with a disubstituted phenyl ring while keeping the 3-(pyrrolidin-1-yl)propoxyl and methoxy groups. As a result, we discovered a much simpler compound with a molecular weight less than 300, **2** (Figure 2), as a SPIN1 inhibitor. Importantly, compared with compound **1**, compound **2** showed approximately 10-fold improvement in potency for SPIN1 (IC_{50} = 338 ± 30 nM (AlphaLISA) and 741 ± 46 nM (FP)) (Figure 3A,B). We determined that compound **2** bound SPIN1 with a K_D value of 390 ± 54 nM using isothermal titration calorimetry (ITC) (Figure 3C). To our delight, **2** did not bind either G9a or GLP using the same ITC experiments (Figures 3D and S3).

Discovery of Compound 3. To improve potency of compound **2**, we replaced the pyrrolidinyl group with an isoindolinyl group, trying to achieve some $\pi-\pi$ stacking interactions in the aromatic cage of the SPIN1 tudor domain II. As what we expected, compared with **2**, the resulting compound **3** (Figure 2) showed >4-fold higher potency for SPIN1 (IC_{50} = 77 ± 3 nM (AlphaLISA) and 243 ± 10 nM (FP)) (Figure 4A), while maintaining a low molecular weight of 341. The potency of compound **3** is comparable to that of A366 (IC_{50} = 72 ± 2 nM (AlphaLISA) and 207 ± 10 nM (FP)) (Figure S1), a G9a/GLP inhibitor[42] whose SPIN1 activity was previously reported by us.[23] We next assessed the binding affinity of compound **3** to SPIN1 using ITC and found that it bound SPIN1 with a K_D value of 91 ± 4 nM (Figure 4B left panel), which is consistent with its potency in biochemical assays. The molar ratio of 1 was observed, suggesting that compound **3** likely bound only one out of three tudor domains of SPIN1. Importantly, similar to compound **2**, compound **3** did not bind either G9a or GLP in ITC experiments (Figure

DOI: 10.1021/acs.jmedchem.9b00522
J. Med. Chem. 2019, 62, 8996−9007

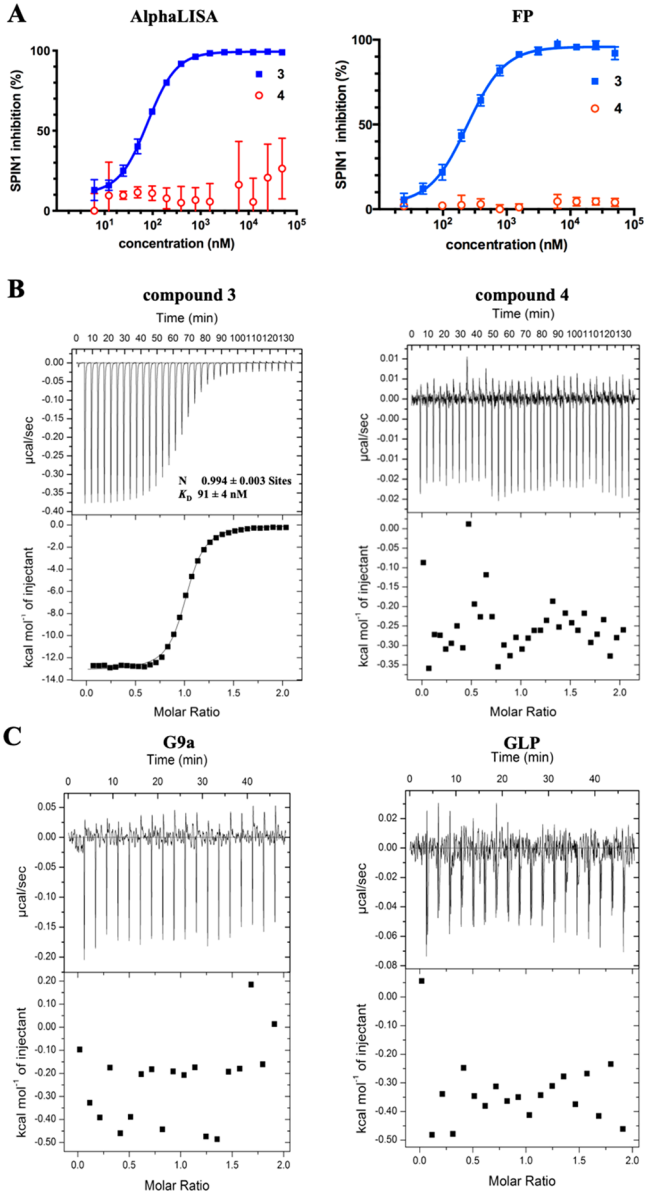

Figure 4. Compound **3** is a potent SPIN1 inhibitor. (A) Compound **3**, but not compound **4**, potently inhibited the interactions between SPIN1 and H3K4me3 with IC_{50} values of 77 ± 3 nM in AlphaLISA assay (n = 3) and 243 ± 10 nM in FP assay (n = 3). (B) Compound **3** bound SPIN1 with a K_D value of 91 ± 4 nM (n = 3) while compound **4** did not bind SPIN1 in ITC experiments. (C) Compound **3** did not bind either G9a or GLP in ITC experiments.

4C). In addition, compound **3** showed moderate binding affinities (ranging from 170 nM to 1.7 μM) to other closely related SPIN subfamily members (SPIN2B, SPIN3, and SPIN4) in ITC experiments (Figure S4), suggesting similar domain architectures and binding modes amongst the SPIN subfamily members.[43−45] To further assess its selectivity, we tested compound **3** against 33 MTs (including G9a and GLP) and 5 acetyltransferases and found that it did not significantly inhibit these MTs and acetyltransferases at up to 50 μM (Figure 5A and Table S1). In addition, we assessed selectivity of compound **3** against 20 methyllysine, methylarginine, and acetyllysine reader proteins using a thermal shift assay and found that compound **3** did not induce a significant thermal shift for any of the 20 reader proteins at 20 or 200 μM (Figure 5B and Table S2). Thus, compound **3** is selective over a broad range of epigenetic proteins.

Determination of the Cocrystal Structure of Compound 3 in the Complex with SPIN1. We next solved the X-ray crystal structure of SPIN1 in the complex with compound **3** at 1.6 Å resolution (PDB code: 6QPL, Figure 6, and Table S3). As illustrated in Figure 6A, compound **3** only occupied the SPIN1 tudor domain II, which recognizes H3K4me3. As expected, the isoindolinyl group occupied the aromatic cage (Figure 6B,C). The protonated amino group in the isoindolinyl group not only formed a hydrogen bond (H-bond) with Y179 but also interacted with Y170, W151, and F141 in the aromatic cage through cation−π interactions (Figure 6C). The phenyl ring of the isoindoline group interacted with W151 through π−π stacking, which may explain the increased potency of compound **3** over compound **2** (Figure 6C). Besides these important interactions formed by the isoindolinyl group, two aminomethylene side chains formed a few critical H-bonds. The amino group of the 3-aminomethylene side chain formed a H-bond with D95 on the loop of the tudor domain I of SPIN1 (Figure 6C). The amino group of the 5-aminomethylene side chain formed a direct H-bond with D184 on the α-helix of tudor domain II and two water-mediated H-bonds with M140 and D189. Disrupting these H-bond interactions by switching the 5-aminomethylene group of compound **3** to an amido group resulted in a structurally similar but inactive compound, **4** (Figure 2), which was completely inactive in the SPIN1 AlphaLISA and FP assays (Figure 4A). In addition, compound **4** did not show detectable binding affinity to SPIN1 in ITC experiments (Figure 4B right panel). Thus, compound **4** could be used as a negative control in chemical biology studies.

Evaluation of Compound 3 in Cellular Assays. Using a NanoBRET target engagement assay,[46] we next demonstrated that compound **3** can engage SPIN1 in cells. As illustrated in Figure 7A,B, compound **3**, but not compound **4**, reduced the interaction between SPIN1 and histone H3 in U2OS cells in a concentration-dependent manner with an IC_{50} value of 3.2 ± 0.7 μM. Thus, compound **3** is cell permeable and can effectively engage SPIN1 in cells. Finally, we assessed off-target toxicity of compound **3** in two transformed cell lines, C2C12 and 293T, and one normal human primary fibroblasts cell line, HFF-1. We found that compound **3** was not toxic to these cells at up to 30 μM (Figure 7C). Thus, compound **3** is a useful tool compound for cellular studies.

Chemical Synthesis. Compounds **2**, **3**, and **4** were synthesized using the synthetic routes shown in Schemes 1−3.

The preparation of compound **2** was started from 3,5-dibromo-2-methoxyphenol (**5**).[47] Protection of the phenol group using benzyl bromide under basic conditions provided benzyl ether intermediate **6**. Next, the dibromo groups on the phenyl ring were converted to dicyano groups under Rosenmund−von Braun reaction conditions, resulting in intermediate **7**. Benzyl ether deprotection under palladium-catalyzed hydrogenation conditions provided phenol **8**, which was subsequently converted to 3-chloropropyl ether **9**. Substitution of the chloro group with pyrrolidine in the presence of potassium iodide yielded intermediate **10**. Lastly, reduction of the dicyano groups under Raney nickel-mediated hydrogenation provided compound **2** (Scheme 1).

Compound **3** was synthesized following similar procedures for preparation of compound **2**. Briefly, isoindoline substitution of the chloro group of intermediate **9** yielded

DOI: 10.1021/acs.jmedchem.9b00522
J. Med. Chem. 2019, 62, 8996−9007

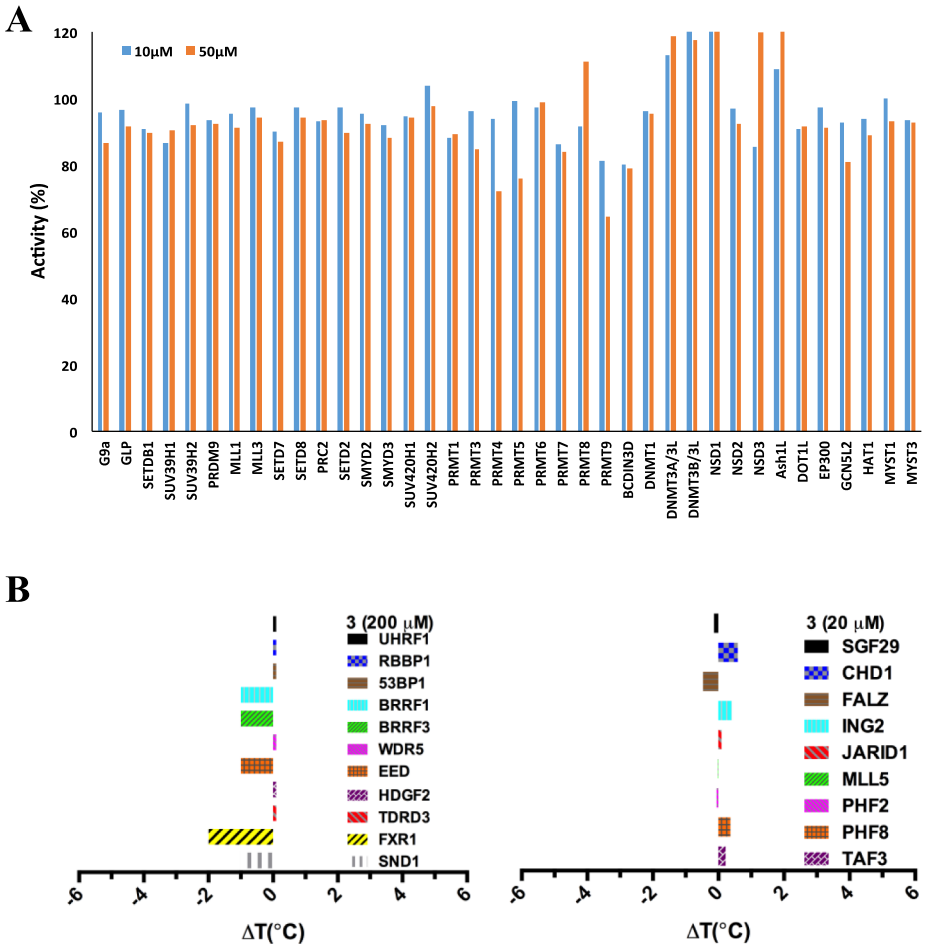

Figure 5. Compound **3** is a selective SPIN1 inhibitor. (A) Compound **3** did not significantly inhibit the enzymatic activity of 33 MTs and 5 acetyltransferases at 10 μM (blue) and 50 μM (red). (B) Compound **3** did not induce significant thermal shifts for 20 methyllysine, methylarginine and acetyllysine reader proteins at 20 μM or 200 μM in thermal shift assays (n = 2).

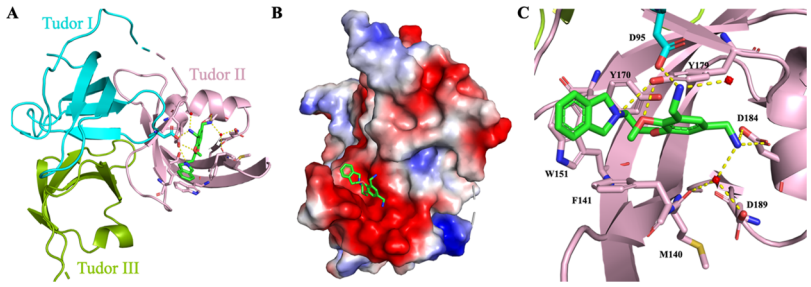

Figure 6. Crystal structure of the SPIN1−compound **3** complex. (A) Compound **3** (green) occupies the tudor domain II (pink) of SPIN1. (B) Electrostatic potential surface view of the structure, ranging from −6 kT/e (red) to +6 kT/e (blue). (C) Close-up view of the SPIN1−compound **3** complex structure with key ligand−protein interactions. Yellow dashes, hydrogen bonds. Red balls, water molecules.

compound **11**. The dicyano groups were subsequently reduced to diaminomethylene groups to afford compound **3** (Scheme 2).

Compound **4** was prepared from commercially available compound **12**. The carboxylic acid and phenolic hydroxyl groups of **12** were simultaneously protected as benzyl ester and benzyl ether groups, respectively, to provide intermediate **13**. The bromo group of **13** was substituted with the cyano group using the Rosenmund−von Braun reaction to yield intermediate **14**. After the hydrolysis of the benzyl ester under basic conditions, the resulting carboxylic acid was activated as acid chloride, which was subsequently converted to amide **16** in the presence of ammonium hydroxide aqueous solution. The benzyl ether was deprotected to provide intermediate **17** with a free phenol group, which was converted to the 3-isoindolinylpropyl ether product **4** in three steps (Scheme 3), using the similar reaction sequences for the preparation of compounds **2** and **3**.

CONCLUSIONS

In summary, we optimized compound **1**, a weak SPIN1 but highly potent G9a/GLP inhibitor, into compound **3**, a potent

DOI: 10.1021/acs.jmedchem.9b00522
J. Med. Chem. 2019, 62, 8996−9007

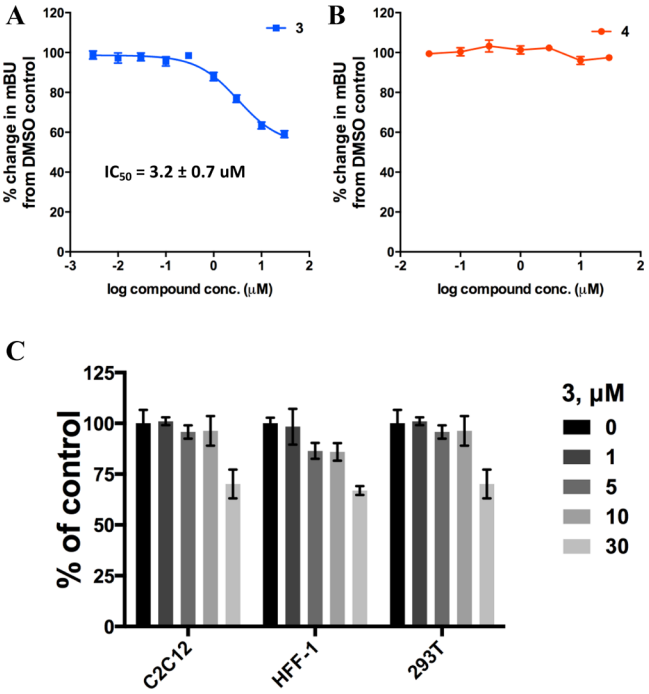

Figure 7. Compound **3** binds SPIN1 in cells and shows no cytotoxicity. (A) Compound **3** disrupted the interaction between SPIN1 and histone H3 (IC_{50} = 3.2 ± 0.7 μM (n = 4)) in U2OS cells in a NanoBRET assay. (B) Compound **4** was inactive in the NanoBRET assay (n = 3). (C) Compound **3** was not toxic to C2C12 and 293T cell lines or primary fibroblasts HFF1, at up to 30 μM (n = 3). Indicated cell lines were cultured in the presence of indicated concentrations of compound **3** for 6 days. Cell viability was measured using Alamar blue.

and selective fragment-like inhibitor of SPIN1. Compound **3** displayed high potency in SPIN1 biochemical assays (IC_{50} = 77 nM (AlphaLISA) and 243 nM (FP)) and high binding affinity to SPIN1 (K_D = 91 nM) by ITC. Compound **3** was completely inactive against G9a and GLP and selective for SPIN1 over a broad range of epigenetic proteins. We also obtained an X-ray crystal structure of SPIN1 in the complex with compound **3**, which confirmed that compound **3** occupied tudor domain II of SPIN1. Based on the cocrystal structure, we designed compound **4**, a close analogue of compound **3** as a negative control, which was indeed inactive in SPIN1 biochemical and biophysical assays. We demonstrated that compound **3**, but not the negative control compound **4**, engaged SPIN1 in cells using a NanoBRET assay, and compound **3** was not toxic in the nontumorigenic cells evaluated. Thus, compound **3** and compound **4** are a pair of useful tool compounds for investigating biological functions and disease associations of SPIN1. Remarkably, compound **3** achieved high potency and selectivity for SPIN1 by targeting a single methyllysine reader domain. These results have demonstrated that it is feasible to generate potent, selective, and cell-active inhibitors by targeting a single tudor domain and paved the way for discovering improved inhibitors of methyllysine reader proteins.

EXPERIMENTAL SECTION

Chemistry General Procedures. High-performance liquid chromatography (HPLC) spectra for compounds were acquired using an Agilent 1200 Series system with a DAD detector. Chromatography was performed on a 2.1 × 150 mm Zorbax 300SB-C_{18} 5 μm column with water containing 0.1% formic acid as solvent A and acetonitrile containing 0.1% formic acid as solvent B at a flow rate of 0.4 mL/min. The gradient program was as follows: 1% B (0−1 min), 1−99% B (1−4 min), and 99% B (4−8 min). Ultra-performance liquid chromatography (UPLC) spectra for compounds were acquired using a Waters Acquity I-Class UPLC system with a PDA detector. Chromatography was performed on a 2.1 × 30 mm ACQUITY UPLC BEH C_{18} 1.7 μm column with water containing 3% acetonitrile, 0.1% formic acid as solvent A and acetonitrile containing 0.1% formic acid as solvent B at a flow rate of 0.8 mL/min. The gradient program was as follows: 1−99% B (1−1.5 min), and 99−1% B (1.5−2.5 min). High-resolution mass spectra (HRMS) data were acquired in the positive ion mode using Agilent G1969A API-TOF with an electrospray ionization (ESI) source. Nuclear magnetic resonance (NMR) spectra were acquired on either a Bruker DRX-600 spectrometer (600 MHz ^{1}H) or a Bruker DXI 800 MHz spectrometer (800 MHz ^{1}H, 200 MHz ^{13}C). Chemical shifts are reported in ppm (δ). Preparative HPLC was performed on Agilent Prep 1200 series with an UV detector set to 254 nm. Samples were injected into a Phenomenex Luna 75 × 30 mm, 5 μm, C_{18} column at room temperature. The flow rate was 40 mL/min. A linear gradient was used with 10% (or 50%) of MeOH (A) in H_2O [with 0.1% trifluoroacetic acid (TFA)] (B) to 100% of MeOH (A). HPLC and UPLC were used to establish the purity of target compounds. All final compounds had >95% purity using the HPLC and UPLC methods described above. Compounds **2** and **3** were tested in biological assays in their HCl salt forms and compound **4** in its CF_3CO_2H salt form.

(4-Methoxy-5-(3-(pyrrolidin-1-yl)propoxy)-1,3-phenylene)-dimethanamine (2). Compound **2** was synthesized from the intermediate **6** following the procedures described below. To a solution of **10** (127 mg, 0.32 mmol) in MeOH (2 mL) was added Raney Ni (50 mg), followed by aqueous ammonia solution (0.1 mL). The mixture was stirred under a hydrogen atmosphere (1 atm) for 12 h, before the insoluble solid was filtered. The filtrate was collected and concentrated. The resulting residue was purified by prep-HPLC to

Scheme 1. Synthesis of Compound 2[a]

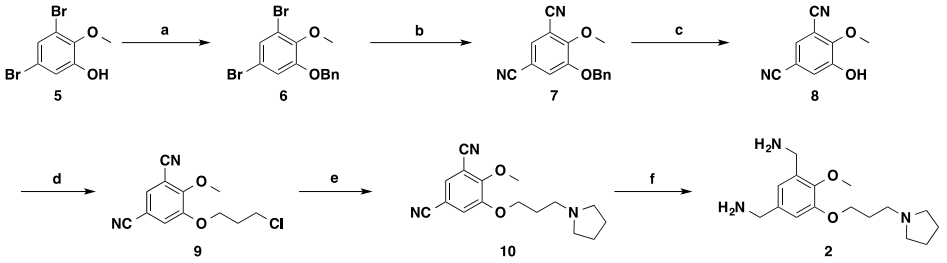

[a]Reagent and conditions: (a) BnBr, K_2CO_3, DMF, rt, 12 h, 90%; (b) CuCN, NMP, 170 °C, 18 h, 40%; (c) H_2 (1 atm), 10% Pd/C, EtOAc, rt, 5 h; (d) 1-bromo-3-chloropropane, DMF, rt, 12 h, 60% in 2 steps; (e) pyrrolidine, K_2CO_3, KI, DMF, 60 °C, 12 h, 80%; (f) H_2 (1 atm), Raney Ni, NH_4OH, MeOH, rt, 12 h, 70%.

DOI: 10.1021/acs.jmedchem.9b00522
J. Med. Chem. 2019, 62, 8996−9007

Scheme 2. Synthesis of Compound 3[a]

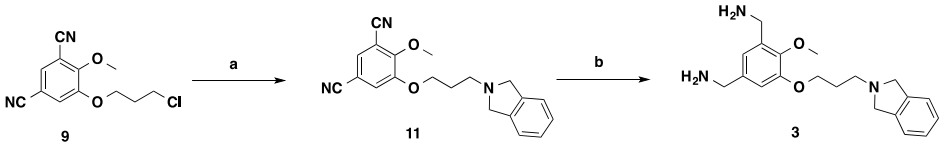

[a]Reagent and conditions: (a) isoindoline, K_2CO_3, KI, DMF, 60 °C, 12 h, 60%; (b) H_2 (1 atm), Raney Ni, NH_4OH, MeOH, rt, 12 h, 65%.

Scheme 3. Synthesis of Compound 4[a]

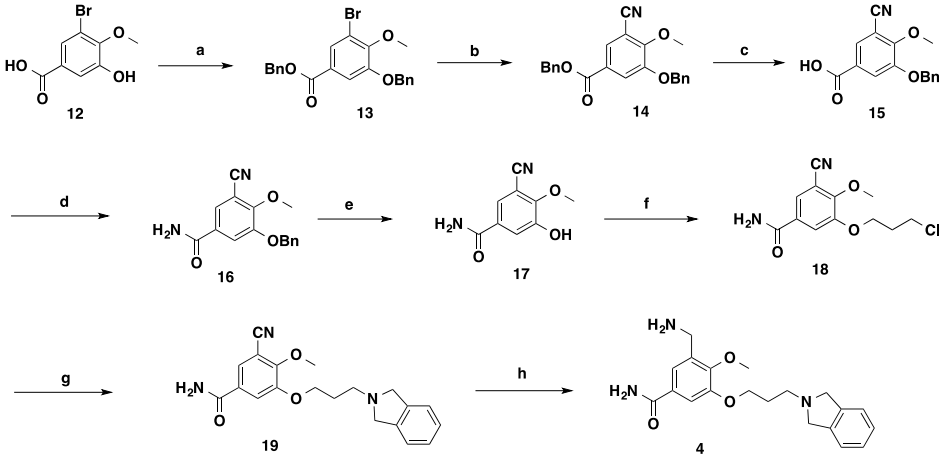

[a]Reagent and conditions: (a) BnBr, K_2CO_3, DMF, rt, 12 h, 91%; (b) CuCN, NMP, 170 °C, 18 h, 54%; (c) NaOH, MeOH, H_2O, rt, 2 h. (d) $(COCl)_2$, DMF, CH_2Cl_2, rt, 1 h; NH_4OH, 0 °C, 1 h, 41% in 3 steps; (e) H_2 (1 atm), 10% Pd/C, EtOAc, rt, 5 h; (f) 1-bromo-3-chloropropane, DMF, rt, 12 h, 55% in 2 steps; (g) isoindoline, K_2CO_3, KI, DMF, 60 °C, 12 h, 61%; (h) H_2 (1 atm), Raney Ni, NH_4OH, MeOH, rt, 12 h, 72%.

yield the title compound as brown oil (90 mg, 70% yield). ^{1}H NMR (600 MHz, CD_3OD): δ 7.38 (s, 1H), 7.16 (s, 1H), 4.28 (t, J = 5.5 Hz, 2H), 4.16 (s, 2H), 4.14 (s, 2H), 4.01 (s, 3H), 3.82−3.69 (m, 2H), 3.52−3.44 (m, 2H), 3.23−3.13 (m, 2H), 2.41−2.32 (m, 2H), 2.26−2.16 (m, 2H), 2.14−2.04 (m, 2H). HPLC >95%, t_R = 1.24 min. HRMS (ESI-TOF) m/z: $[M + H]^+$ calcd for $C_{16}H_{28}N_3O_2$, 294.2176; found, 294.2150.

(5-(3-(Isoindolin-2-yl)propoxy)-4-methoxy-1,3-phenylene)-dimethanamine (3). Compound **3** was synthesized from the intermediate of **11** according to the procedures for the preparation of **2** as brown oil (65% yield). ^{1}H NMR (600 MHz, CD_3OD): δ 7.49−7.42 (m, 4H), 7.40 (s, 1H), 7.15 (s, 1H), 5.02 (d, J = 13.8 Hz, 2H), 4.68 (d, J = 13.9 Hz, 2H), 4.33 (t, J = 5.8 Hz, 2H), 4.16 (s, 2H), 4.14 (s, 2H), 4.01 (s, 3H), 3.74 (t, J = 7.8 Hz, 2H), 2.50−2.38 (m, 2H). ^{13}C NMR (200 MHz, MeOD): δ 151.60, 148.24, 133.57, 129.30, 128.79, 126.98, 122.93, 122.60, 115.77, 65.82, 60.35, 58.51, 52.32, 42.47, 38.30, 25.46. HPLC >95%, t_R = 1.31 min. HRMS (ESI-TOF) m/z: $[M + H]^+$ calcd for $C_{20}H_{28}N_3O_2$, 342.2176; found, 342.2145.

3-(Aminomethyl)-5-(3-(isoindolin-2-yl)propoxy)-4-methoxybenzamide (4). Compound **4** was synthesized from intermediate **19** according to the procedures for the preparation of compound **2** as brown oil (72% yield). ^{1}H NMR (600 MHz, CD_3OD): δ 7.67 (s, 1H), 7.59 (s, 1H), 7.48−7.44 (m, 4H), 5.08−4.94 (m, 2H), 4.77−4.58 (m, 2H), 4.32 (t, J = 5.7 Hz, 2H), 4.22 (s, 2H), 3.99 (s, 3H), 3.78 (d, J = 7.8 Hz, 2H), 2.42−2.32 (m, 2H). ^{13}C NMR (200 MHz, MeOD): δ 169.50, 152.05, 148.83, 133.55, 129.93, 128.83, 126.40, 122.60, 121.41, 112.85, 70.05, 58.60, 55.26, 52.59, 38.20, 26.39. UPLC >95%, t_R = 0.66 min. HRMS (ESI-TOF) m/z: $[M + H]^+$ calcd for $C_{20}H_{26}N_3O_3$, 356.1969; found, 356.1994.

1-(Benzyloxy)-3,5-dibromo-2-methoxybenzene (6). To a solution of **5**[47] (1.71 g, 6.1 mmol) in dimethylformamide (DMF) (10 mL) was added K_2CO_3 (1.60 g, 11.6 mmol), followed by benzyl bromide (0.89 mL, 7.5 mmol). The resulting suspension was stirred at rt for 12 h, before water (10 mL) was added to quench the reaction. The mixture was extracted with ether (3 × 20 mL). The combined organic phase was dried with anhydrous Na_2SO_4, filtered, and concentrated under reduced pressure. The resulting residue was purified by flash chromatography to yield the title compound as the white solid (2.05 g, 90% yield). ^{1}H NMR (600 MHz, $CDCl_3$): δ 7.49−7.36 (m, 5H), 7.33 (s, 1H), 7.08 (s, 1H), 5.12 (s, 2H), 3.89 (s, 3H).

5-(Benzyloxy)-4-methoxyisophthalonitrile (7). To a solution of **6** (2.05 g, 5.5 mmol) in N-Methyl-2-pyrrolidone (NMP) (10 mL) was added CuCN (1.08 g, 12.1 mmol). The mixture was heated in a sealed tube for 18 h. After cooling to room temperature, aqueous ammonia solution (2 mL) was added. The reaction was extracted with ether (3 × 20 mL). The combined organic phase was dried with anhydrous Na_2SO_4, filtered, and concentrated. The residue was purified by flash chromatography to yield the title compound as colorless oil (580 mg, 40% yield). ^{1}H NMR (600 MHz, $CDCl_3$): δ 7.49 (s, 1H), 7.48−7.40 (m, 5H), 7.37 (s, 1H), 5.18 (s, 2H), 4.18 (s, 3H). UPLC >95%, t_R = 1.62 min.

5-(3-Chloropropoxy)-4-methoxyisophthalonitrile (9). To a solution of **7** (580 mg, 2.2 mmol) in ethyl acetate (10 mL) was added 10% palladium on carbon (50 mg). The mixture was stirred in a hydrogen atmosphere (1 atm) for 5 h, before being filtered. The filtrate was concentrated. The resulting residue was dissolved in DMF (5 mL). To the resulting solution was added K_2CO_3 (455 mg, 3.3 mmol), followed by 1-bromo-3-chloropropane (0.43 mL, 4.4 mmol). The mixture was stirred at room temperature for 12 h, before water was added to quench the reaction. The mixture was extracted with ether (3 × 20 mL). The combined organic phase was combined, dried over anhydrous Na_2SO_4, and concentrated. The resulting residue was purified by flash chromatography to yield the title compound as colorless oil (335 mg, 60% yield). ^{1}H NMR (600 MHz, $CDCl_3$): δ 7.50 (s, 1H), 7.37 (s, 1H), 4.24 (t, J = 5.8 Hz, 2H), 4.16 (s, 3H), 3.78 (t, J = 6.1 Hz, 2H), 2.39−2.32 (m, 2H). UPLC >95%, t_R = 1.47 min.

4-Methoxy-5-(3-(pyrrolidin-1-yl)propoxy)isophthalonitrile (10). To a solution of **9** (100 mg, 0.4 mmol) in DMF (2 mL) was added pyrrolidine (84 μL, 1 mmol), K_2CO_3 (140 mg, 1 mmol), and KI (15 mg, 0.1 mmol). The resulting suspension was heated at 60 °C

DOI: 10.1021/acs.jmedchem.9b00522
J. Med. Chem. 2019, 62, 8996−9007

for 12 h. After cooling to room temperature, the reaction was quenched with water (5 mL) and extracted with CH_2Cl_2 (3 × 5 mL). The combined organic phase was dried over anhydrous Na_2SO_4, filtered, and concentrated. The resulting residue was purified by pre-HPLC to yield the title compound as brown oil (127 mg, 80% yield). ^{1}H NMR (600 MHz, CD_3OD): δ 7.74 (s, 1H), 7.71 (s, 1H), 4.26 (t, J = 5.7 Hz, 2H), 4.16 (s, 3H), 3.82−3.69 (m, 2H), 3.49−3.41 (m, 2H), 3.22−3.11 (m, 2H), 2.40−2.29 (m, 2H), 2.28−2.17 (m, 2H), 2.14−2.00 (m, 2H). UPLC >95%, t_R = 0.95 min.

5-(3-(Isoindolin-2-yl)propoxy)-4-methoxyisophthalonitrile (11). Compound **11** was synthesized from intermediate **9** according to the procedures for the preparation of **10** as brown oil (60% yield). ^{1}H NMR (600 MHz, CD_3OD): δ 7.72 (dd, J = 3.8, 1.7 Hz, 2H), 7.47−7.44 (m, 4H), 5.00 (br, 2H), 4.66 (br, 2H), 4.31 (t, J = 5.8 Hz, 2H), 4.14 (s, 3H), 3.72−3.69 (m, 2H), 2.49−2.37 (m, 2H). HPLC >95%, t_R = 1.24 min.

Benzyl 3-(Benzyloxy)-5-bromo-4-methoxybenzoate (13). To a solution of 3-bromo-5-hydroxy-4-methoxybenzoic acid (1.1 g, 4.4 mmol) in DMF (12 mL) was added benzyl bromide (1.1 mL, 9.2 mmol) and K_2CO_3 (1.6 g, 11.3 mmol). The mixture was stirred at room temperature for 12 h, before being quenched with water. The mixture was extracted with ether (3 × 30 mL). The combined organic phase was dried over anhydrous Na_2SO_4, filtered, and concentrated. The resulting residue was purified by flash chromatography to yield the title compound as the white solid (1.7 g, 91% yield).

Benzyl 3-(Benzyloxy)-5-cyano-4-methoxybenzoate (14). Compound **14** was synthesized from intermediate **13** according to the procedures for the preparation of **7** as the brown solid (54% yield). ^{1}H NMR (600 MHz, $CDCl_3$): δ 7.92 (d, J = 1.8 Hz, 1H), 7.60 (d, J = 1.8 Hz, 1H), 7.57−7.54 (m, 2H), 7.50−7.46 (m, 2H), 7.46−7.34 (m, 6H), 5.39 (s, 2H), 5.15 (s, 2H), 3.94 (s, 3H). UPLC >95%, t_R = 1.74 min.

3-(Benzyloxy)-5-cyano-4-methoxybenzamide (16). To a solution of **14** (460 mg, 1.2 mmol) in MeOH (5 mL) was added aqueous NaOH (1.5 mL, 1 N, 1.5 mmol) solution. The solution was stirred at room temperature for 2 h, before being acidified with aqueous HCl (2 mL, 1 N, 2 mmol). The resulting suspension was filtered. The collected solid was dried and used for the next step without further purification. The crude acid (370 mg, 1.3 mmol) was dissolved in CH_2Cl_2 (5 mL). To the resulting solution was added $(COCl)_2$ (0.22 mL, 2.6 mmol) and DMF (several drops). The solution was stirred at room temperature for 1 h, before being concentrated. The resulting residue was dissolved in CH_2Cl_2 (5 mL). To the solution was added aqueous ammonia solution (1 mL, 28%, 14.8 mmol) at 0 °C. The mixture was stirred for 1 h at 0 °C before being poured into a separatory funnel. The organic phase was collected. The aqueous phase was extracted with CH_2Cl_2 (2 × 5 mL). The organic phase was combined, dried over Na_2SO_4, filtered, and concentrated. The resulting residue was purified by flash chromatography to yield the title compound as the brown solid (140 mg, 41% in 2 steps). ^{1}H NMR (600 MHz, $CDCl_3$): δ 7.74 (d, J = 1.9 Hz, 1H), 7.67 (d, J = 1.9 Hz, 1H), 7.45−7.41 (m, 2H), 7.35−7.25 (m, 3H), 5.30 (s, 2H), 4.69 (s, 2H), 3.96 (s, 3H). UPLC >95%, t_R = 1.29 min.

3-(3-Chloropropoxy)-5-cyano-4-methoxybenzamide (18). Compound **18** was synthesized from intermediate **16** according to the procedures for the preparation of **9** as the off-white solid (55% yield in 2 steps). ^{1}H NMR (600 MHz, CD_3OD): δ 7.74 (s, 1H), 7.69 (s, 1H), 4.41 (t, J = 5.6 Hz, 2H), 4.26 (s, 2H), 3.94 (s, 3H), 3.83 (t, J = 6.2 Hz, 2H), 2.26−2.17 (m, 2H). UPLC >95%, t_R = 1.20 min.

3-Cyano-5-(3-(isoindolin-2-yl)propoxy)-4-methoxybenzamide (19). Compound **19** was synthesized from intermediate **18** according to the procedures for the preparation of **11** as brown oil (61% yield). ^{1}H NMR (600 MHz, CD_3OD): δ 7.86 (d, J = 2.0 Hz, 1H), 7.79 (d, J = 1.9 Hz, 1H), 7.56−7.35 (m, 4H), 5.06−4.96 (m, 2H), 4.72−4.65 (m, 2H), 4.46 (t, J = 5.6 Hz, 2H), 4.00 (s, 3H), 3.89−3.79 (m, 2H), 2.43−2.27 (m, 2H). UPLC >95%, t_R = 0.90 min.

Crystallization and X-ray Cocrystal Structure Determination. $SPIN1_{Pro49-Ser262}$ was crystallized with compound **3** at 4 °C using the sitting drop vapor diffusion method. SPIN1 was incubated with 1.5 mM of compound **3** using 39 mg/mL protein, and crystals appeared in drops consisting of 75 nL protein compound mixture and 75 nL precipitant consisting of 60% 2-Methyl-2,4-pentanediol (MPD), and 0.1 M SPG (succinate, phosphate, and glycine) buffer pH 6.0. A 1.6 Å resolution dataset was collected on beamline I04 at Diamond Light Source UK. The dataset was processed, scaled, and merged at the Diamond Light Source using Xia2.[48−52]

The structure was solved by molecular replacement using PHASER and SPIN1 PDB ID 6I8L as a search model. The structure was refined in PHENIX[53] with electron density map inspections and model improvement in COOT[54] and terminated when there were no significant changes in the R_{work} and R_{free} values, and inspection of the electron density map suggested that no further corrections or additions were justified. Statistics for data collection and refinement are shown in Table S3. Structural analyses were performed with PyMOL (http://www.pymol.org) and the coordinates deposited in PDB with the ID 6QPL.

SPIN1 FP Assay. FP experiments were performed as previously described.[23] The compounds were measured as a 12-point serial dilution with concentrations ranging from 24 nM to 50 μM, resulting in a final dimethyl sulfoxide (DMSO) concentration of 0.5%. Blank values were measured in six wells on the first and last row of the assay plate. Each concentration as well as positive and negative controls were tested in triplicates. The incubation time was modified to 30 min.

SPIN1 AlphaLISA Assay. AlphaLISA experiments were performed as previously described.[23] The compounds were measured as a 14-point serial dilution with concentrations ranging from 6.1 nM to 50 μM, resulting in a final DMSO concentration of 0.5%. Blank values were measured in seven wells on the first and last row of the assay plate. Each concentration as well as positive and negative controls were done in triplicates. The incubation time after addition of the beads was modified to 90 min.

IC_{50} values were calculated using the combined inhibition values of two independent experiments and applying a sigmoidal dose−response fit (variable slope) using GraphPad Prism (version 7).

G9a and GLP ITC Experiments. ITC measurements were made at 25 °C on a MicroCal ITC200 Instrument (Malvern Instruments). Coconcentrated G9a−SAM and GLP−SAM (protein/SAM molar ratio of 1:5) were diluted at 35 μM in ITC buffer [50 mM Tris (pH 8.0), 150 mM NaCl] supplemented with 1% DMSO. Small molecule compounds were dissolved in DMSO at 50 mM and diluted to 0.5 mM in ITC buffer with a final DMSO concentration of 1%. Binding constants were calculated by fitting the data using the ITC data analysis module in Origin 7.0 (OriginLab Corp.).

SPIN1 ITC Experiments. ITC experiments were performed at 20 °C with a MicroCal VP-ITC microcalorimeter (GE Healthcare) by injection of 8 μL of compound solution (100−300 μM) during 16 s into the sample cell containing 10 μM of His−SPIN1(49−262) in ITC assay buffer. DMSO was adapted in a syringe and sample cell to 0.1−0.3%. A total of 33 injections were performed with a spacing of 240 s and a reference power of 10 μcal s^{-1}.

Automated baseline assignment and peak integration were performed with NITPIC version 1.0.1.[55] Isotherms were plotted by global analysis of multiple titrations, with the simplex algorithm, with SEDPHAT version 10.58d.[56] Isotherms were subsequently validated by two-dimensional error surface projections at P levels of 0.68 and 0.95 in SEDFIT.[57]

Other SPIN Subfamily ITC Experiments. Purified protein was diluted to 10−30 μM in ITC buffer (100 mM NaCl, 20 mM Tris, pH 8.0) and then dialyzed against a 1000 times excess of ITC buffer at 4 °C overnight using D-Tube Dialyzer tubes (Merck/Sigma-Aldrich) with a 3.5 kDa molecular weight cut-off. The dialyzed sample was then centrifuged at 14 000 rpm for 10 min in a standard chilled benchtop centrifuge at 4 °C. Protein concentration was then verified via absorption at 280 nm using a NanoDrop ND1000 Spectrophotometer. Compounds were diluted to 200 μM in ITC buffer. Experiments were performed on a NanoITC Standard Volume instrument (960 μL cell volume, 250 μL syringe volume; TA Instruments) using direct titration (protein in cell, compound in syringe) at 20 °C, a stir rate of 350 rpm, and an injection rate of 50

DOI: 10.1021/acs.jmedchem.9b00522
J. Med. Chem. 2019, 62, 8996−9007

ms/step (~1.4 μL/s). An initial injection of 3.7 μL followed after 200 s by 30 injections of 7.96 μL spaced at 300 s. Data were analyzed using an independent fit model with the NanoAnalyse software (TA Instruments, version 3.8.0).

Thermal Shift (T_m) Assay. Compounds were dispensed on white PCR plates using an Echo 550 acoustic liquid dispenser to a final concentration of 20 or 200 μM with two technical replicates per concentration per protein. Protein in T_m shift buffer (20 mM HEPES, 500 mM NaCl, pH 7.5, SYPRO orange dye at 1:1000 dilution from purchased stock) was added at 2 μM final concentration. The lower concentrations were back-filled with DMSO to the same amount dispensed as for the highest concentration, and DMSO-only controls were also included (n = 4 per protein). Experiments were performed on Agilent Mx3005P qPCR machines (reaction volume 20 μL) or Roche Lightcycler 480 (reaction volume 5 μL). The temperature gradient was run from 25 to 95 °C over 25 min. Melting temperatures T_m were estimated as the inflection point of a Boltzmann equation fitted to the fluorescence intensity $I(T)$ from the onset (I_{onset}) to the peak (I_{peak}) of intensity where S is the slope of the curve

$$I(T) = I_{onset} + (I_{peak} - I_{onset})/1 + e^{((T_m - T)/S)}$$

Shifts in unfolding (DT_m) were then calculated as the difference between the individual T_m from the mean of the DMSO controls.

MT and Acetyltransferase Selectivity Assays. The effect of compound **3** on activities of 33 MTs and 5 acetyltransferases was assessed using activity assays as previously described.[58]

NanoBRET Assay. U20S cells (2.8×10^5) were plated in each well of a 6-well plate. After 6 h cells were cotransfected with C-terminal HaloTag–histone 3.3 (NM_002107) and an N-terminal NanoLuciferase fusion of full length SPIN1 at a 1:500 (NanoLuc to HaloTag) ratio, respectively, with a FuGENE HD transfection reagent. 16 h post-transfection, cells were collected, washed with phosphate-buffered saline, and exchanged into media containing phenol red-free Dulbecco's modified Eagle's medium (DMEM) and 4% fetal bovine serum (FBS) in the absence (control sample) or the presence (experimental sample) of the 100 nM NanoBRET 618 fluorescent ligand (Promega). Cells were then replated in a 384-well assay white plate (Greiner #3570) at 2.7×10^3 cells per well. Compound **3** and compound **4** were then added directly to media at final concentrations 0–30 μM or an equivalent amount of DMSO as a vehicle control, and the plates were incubated for 24 h at 37 °C in the presence of 5% CO_2. The NanoBRET Nano-Glo substrate (Promega) was added to both control and experimental samples at a final concentration of 10 μM. Readings were performed within 10 min using ClarioSTAR (BMG Labtech). A corrected BRET ratio was calculated and is defined as the ratio of the emission at 610 nm/460 nm for experimental samples minus the emission at 610 nm/460 nm for control samples (without NanoBRET fluorescent ligand). BRET ratios are expressed as milliBRET units (mBU), where 1 mBU corresponds to the corrected BRET ratio multiplied by 1000. The assay was further validated by the domain-specific site directed mutagenesis (Y170A) ablating peptide and ligand binding.

Cell Viability Assay. 293T (gift from Dr. Benchimol), C2C12 (gift from Dr. McPherson), and HFF1 (ATTC) cells were cultured following standard protocols in DMEM (Gibco) 10% FBS (Wisent) and penicillin–streptomycin (Gibco). Cells were seeded in 96-well plates (seeding density: 2000 for HFF-1, 1000 for 293T and 500 for C2C12), recovered for 8 h, and treated with several different concentrations of compound **3** for 6 days. Following cell treatment, cell viability was measured by adding resazurin (Sigma) to the media at 0.01 mg/mL, incubating plates for 2–4 h in a 37 °C CO_2 incubator, and measuring fluorescence at 590 nm on a CLARIOstar microplate reader (BMG Labtech).

Construct Design, Cloning, Expression, and Purification of Human Spindlin Proteins. A plasmid-encoding full-length human SPIN1 was obtained from Source Bioscience (IOH9972-pDEST26) and used as a template to clone $SPIN1_{M26-Ser262}$ and $SPIN1_{P49-S262}$ into the pNIC-CTHF vector with a TEV (tobacco etch virus) cleavable C-terminal His_6 tag. $SPIN1_{G21-S262}$ was cloned into the pNIC-Bio2 vector with a TEV cleavable N-terminal His_{10} tag and a C-terminal biotinylation sequence. $SPI2B_{P45-S258}$, $SPIN3_{M27-S258}$, and $SPIN4_{T36-P249}$ were cloned into the pNIC vector with a TEV cleavable N-terminal His6 tag using templates obtained from the Mammalian Gene Collection and Source Bioscience (SPIN2B: cDNA clone IMAGE id: 6729986, SPIN3 IMAGENE: IRCBp5005F0211Q and SPIN4 IMAGE id 40032302). The recombinant proteins were expressed in a phage-resistant derivative of *Escherichia coli* strain BL21(DE3) carrying the pRARE2 plasmid for rare codon expression. Cells were grown at 37 °C in Terrific broth supplemented with 50 μg/mL kanamycin and 34 μg/mL chloramphenicol, until the culture reached an OD_{600} of 2.0. The temperature was decreased to 18 °C and protein expression induced with 0.1 mM IPTG (isopropyl β-D-thiogalactopyranoside) overnight. Cells were collected by centrifugation and frozen at −80 °C. For purification, cells were resuspended in 50 mM HEPES pH 7.5, 500 mM NaCl, 10 mM imidazole, 5% glycerol, 0.5 mM TCEP, and a protease inhibitor cocktail (Sigma), and lysed by sonication. The cell lysate was clarified by centrifugation, and the proteins were purified by nickel-affinity chromatography (GE Healthcare) using a stepwise gradient of imidazole. This was followed by size exclusion chromatography (Superdex 75 or Superdex 200, GE Healthcare) as previously described.[23] For the ITC assay, aliquots of purified His–SPIN1(49–262) protein were stored at −80 °C in the ITC assay buffer containing 20 mM Tris-HCl (pH 8.0), 200 mM NaCl. For crystallization studies, the histidine tag was removed by incubation with TEV protease at 4 °C overnight, and the TEV protease and the uncleaved proteins were then removed by nickel-affinity chromatography. Proteins were concentrated using an Amicon centrifugal filtration unit, and the mass was verified by ESI time of flight mass spectrometry (ESI-TOF-TOF: Agilent LC/MSD).

Construct Design, Cloning, Expression, and Purification of G9a and GLP Proteins. Human G9a and GLP catalytic domains were cloned, expressed, and purified as previously described.[59]

■ ASSOCIATED CONTENT

Supporting Information

The Supporting Information is available free of charge on the ACS Publications website at DOI: 10.1021/acs.jmedchem.9b00522.

Concentration response curves of A366 and compound **1** in the SPIN1 AlphaLISA and FP biochemical assays; docking model of compound **1** in the complex with SPIN1; binding of compound **2** to GLP by ITC; binding of compound **3** to SPIN2B, SPIN3, and SPIN4 by ITC; ^1H NMR and ^{13}C NMR spectra of compounds **3** and **4**; raw data of the enzymatic inhibition assay against 33 MTs and 5 acetyltransferases; raw data results of the T_m shift assay against 20 methyllysine, methylarginine, and acetyllysine reader proteins; crystallography data and refinement statistics; and description of cell lines for cytotoxicity assays (PDF)

Molecular formula strings (CSV)

Accession Codes

The structure of SPIN1 in the complex with compound **3** has been deposited under PDB ID 6QPL. The authors will release the atomic coordinates and experimental data upon article publication.

■ AUTHOR INFORMATION

Corresponding Authors

*E-mail: udo.oppermann@sgc.ox.ac.uk (U.O.).
*E-mail: roland.schuele@uniklinik-freiburg.de (R.S.).
*E-mail: jian.jin@mssm.edu (J.J.).

ORCID

Cheryl H. Arrowsmith: 0000-0002-4971-3250

DOI: 10.1021/acs.jmedchem.9b00522
J. Med. Chem. 2019, 62, 8996–9007

Paul Brennan: 0000-0002-8950-7646
Manfred Jung: 0000-0002-6361-7716
Udo Oppermann: 0000-0001-9984-5342
Jian Jin: 0000-0002-2387-3862

Author Contributions

[§§]Y.X., H.G., and C.J. contributed equally to this work.

Notes

The authors declare no competing financial interest.

■ ACKNOWLEDGMENTS

R.S. acknowledges support by grants of the European Research Council (ERC AdGrant 322844) and the Deutsche Forschungsgemeinschaft CRC 992, 850, and Schu688/15-1. M.J. thanks the DFG (Deutsche Forschungsgemeinschaft, CRC992) for funding. The SGC is a registered charity (number 1097737) that receives funds from AbbVie, Bayer Pharma AG, Boehringer Ingelheim, Canada Foundation for Innovation, Eshelman Institute for Innovation, Genome Canada, Innovative Medicines Initiative (EU/EFPIA) [ULTRA-DD grant no. 115766], Janssen, Merck KGaA Darmstadt Germany, MSD, Novartis Pharma AG, Ontario Ministry of Economic Development and Innovation, Pfizer, São Paulo Research Foundation-FAPESP, Takeda, and Wellcome [106169/ZZ14/Z]. We acknowledge the Natural Sciences and Engineering Research Council of Canada (NSERC) for a postdoctoral fellowship awarded to D.D. We thank Drs. Benchimol and McPherson for providing 293T and C2C12 cells.

■ ABBREVIATIONS

SPIN1, spindlin 1; GLP, G9a-like protein 1; L3MBTL3, lethal(3) malignant brain tumor-like protein 3; CBX, chromobox; MBT, malignant brain tumor; H3K4me3, trimethylation of lysine 4 on histone H3; H3R8me2, dimethylation of arginine 9 on histone H3; PTMs, post-translational modifications; Wnt, wingless/integrated; TCF, T-cell factor/lymphoid enhancer-binding factor; LE, ligand efficiency; SAR, structure−activity relationship; Alpha, amplified luminescent proximity homogeneous assay; FP, fluorescence polarization; ITC, isothermal titration calorimetry; BRET, bioluminescence resonance energy transfer

■ REFERENCES

(1) Bernstein, B. E.; Meissner, A.; Lander, E. S. The mammalian epigenome. *Cell* **2007**, *128*, 669−681.
(2) Strahl, B. D.; Allis, C. D. The language of covalent histone modifications. *Nature* **2000**, *403*, 41−45.
(3) Rea, S.; Eisenhaber, F.; O'Carroll, D.; Strahl, B. D.; Sun, Z.-W.; Schmid, M.; Opravil, S.; Mechtler, K.; Ponting, C. P.; Allis, C. D.; Jenuwein, T. Regulation of chromatin structure by site-specific histone H3 methyltransferases. *Nature* **2000**, *406*, 593−599.
(4) Kouzarides, T. Chromatin modifications and their function. *Cell* **2007**, *128*, 693−705.
(5) Kaniskan, H. Ü.; Jin, J. Chemical probes of histone lysine methyltransferases. *ACS Chem. Biol.* **2015**, *10*, 40−50.
(6) Kaniskan, H. Ü.; Konze, K. D.; Jin, J. Selective inhibitors of protein methyltransferases. *J. Med. Chem.* **2015**, *58*, 1596−1629.
(7) Kaniskan, H. Ü.; Martini, M. L.; Jin, J. Inhibitors of protein methyltransferases and demethylases. *Chem. Rev.* **2018**, *118*, 989−1068.
(8) Shi, Y.; Lan, F.; Matson, C.; Mulligan, P.; Whetstine, J. R.; Cole, P. A.; Casero, R. A.; Shi, Y. Histone demethylation mediated by the nuclear amine oxidase homolog LSD1. *Cell* **2004**, *119*, 941−953.
(9) Dhalluin, C.; Carlson, J. E.; Zeng, L.; He, C.; Aggarwal, A. K.; Zhou, M.-M.; Zhou, M.-M. Structure and ligand of a histone acetyltransferase bromodomain. *Nature* **1999**, *399*, 491−496.
(10) Su, Z.; Denu, J. M. Reading the combinatorial histone language. *ACS Chem. Biol.* **2016**, *11*, 564−574.
(11) Dawson, M. A.; Kouzarides, T.; Huntly, B. J. P. Targeting epigenetic readers in cancer. *N. Engl. J. Med.* **2012**, *367*, 647−657.
(12) Arrowsmith, C. H.; Bountra, C.; Fish, P. V.; Lee, K.; Schapira, M. Epigenetic protein families: a new frontier for drug discovery. *Nat. Rev. Drug Discovery* **2012**, *11*, 384−400.
(13) Helin, K.; Dhanak, D. Chromatin proteins and modifications as drug targets. *Nature* **2013**, *502*, 480−488.
(14) Højfeldt, J. W.; Agger, K.; Helin, K. Histone lysine demethylases as targets for anticancer therapy. *Nat. Rev. Drug Discovery* **2013**, *12*, 917−930.
(15) Arrowsmith, C. H.; Audia, J. E.; Austin, C.; Baell, J.; Bennett, J.; Blagg, J.; Bountra, C.; Brennan, P. E.; Brown, P. J.; Bunnage, M. E.; Buser-Doepner, C.; Campbell, R. M.; Carter, A. J.; Cohen, P.; Copeland, R. A.; Cravatt, B.; Dahlin, J. L.; Dhanak, D.; Edwards, A. M.; Frederiksen, M.; Frye, S. V.; Gray, N.; Grimshaw, C. E.; Hepworth, D.; Howe, T.; Huber, K. V. M.; Jin, J.; Knapp, S.; Kotz, J. D.; Kruger, R. G.; Lowe, D.; Mader, M. M.; Marsden, B.; Mueller-Fahrnow, A.; Müller, S.; O'Hagan, R. C.; Overington, J. P.; Owen, D. R.; Rosenberg, S. H.; Ross, R.; Roth, B.; Schapira, M.; Schreiber, S. L.; Shoichet, B.; Sundström, M.; Superti-Furga, G.; Taunton, J.; Toledo-Sherman, L.; Walpole, C.; Walters, M. A.; Willson, T. M.; Workman, P.; Young, R. N.; Zuercher, W. J. The promise and peril of chemical probes. *Nat. Chem. Biol.* **2015**, *11*, 536−541.
(16) Smith, S. G.; Zhou, M.-M. The bromodomain: a new target in emerging epigenetic medicine. *ACS Chem. Biol.* **2016**, *11*, 598−608.
(17) James, L. I.; Frye, S. V. Chemical probes for methyl lysine reader domains. *Curr. Opin. Chem. Biol.* **2016**, *33*, 135−141.
(18) Milosevich, N.; Hof, F. Chemical inhibitors of epigenetic methyllysine reader proteins. *Biochemistry* **2016**, *55*, 1570−1583.
(19) Greschik, H.; Schüle, R.; Günther, T. Selective targeting of epigenetic reader domains. *Expert Opin. Drug Discovery* **2017**, *12*, 449−463.
(20) Zaware, N.; Zhou, M.-M. Chemical modulators for epigenome reader domains as emerging epigenetic therapies for cancer and inflammation. *Curr. Opin. Chem. Biol.* **2017**, *39*, 116−125.
(21) James, L. I.; Barsyte-Lovejoy, D.; Zhong, N.; Krichevsky, L.; Korboukh, V. K.; Herold, J. M.; MacNevin, C. J.; Norris, J. L.; Sagum, C. A.; Tempel, W.; Marcon, E.; Guo, H.; Gao, C.; Huang, X.-P.; Duan, S.; Emili, A.; Greenblatt, J. F.; Kireev, D. B.; Jin, J.; Janzen, W. P.; Brown, P. J.; Bedford, M. T.; Arrowsmith, C. H.; Frye, S. V. Discovery of a chemical probe for the L3MBTL3 methyllysine reader domain. *Nat. Chem. Biol.* **2013**, *9*, 184−191.
(22) Stuckey, J. I.; Dickson, B. M.; Cheng, N.; Liu, Y.; Norris, J. L.; Cholensky, S. H.; Tempel, W.; Qin, S.; Huber, K. G.; Sagum, C.; Black, K.; Li, F.; Huang, X.-P.; Roth, B. L.; Baughman, B. M.; Senisterra, G.; Pattenden, S. G.; Vedadi, M.; Brown, P. J.; Bedford, M. T.; Min, J.; Arrowsmith, C. H.; James, L. I.; Frye, S. V. A cellular chemical probe targeting the chromodomains of polycomb repressive complex 1. *Nat. Chem. Biol.* **2016**, *12*, 180−187.
(23) Wagner, T.; Greschik, H.; Burgahn, T.; Schmidtkunz, K.; Schott, A.-K.; McMillan, J.; Baranauskienė, L.; Xiong, Y.; Fedorov, O.; Jin, J.; Oppermann, U.; Matulis, D.; Schüle, R.; Jung, M. Identification of a small-molecule ligand of the epigenetic reader protein Spindlin1 via a versatile screening platform. *Nucleic Acids Res.* **2016**, *44*, No. e88.
(24) Bae, N.; Viviano, M.; Su, X.; Lv, J.; Cheng, D.; Sagum, C.; Castellano, S.; Bai, X.; Johnson, C.; Khalil, M. I.; Shen, J.; Chen, K.; Li, H.; Sbardella, G.; Bedford, M. T. Developing Spindlin1 small-molecule inhibitors by using protein microarrays. *Nat. Chem. Biol.* **2017**, *13*, 750−756.
(25) Zhao, Q.; Qin, L.; Jiang, F.; Wu, B.; Yue, W.; Xu, F.; Rong, Z.; Yuan, H.; Xie, X.; Gao, Y.; Bai, C.; Bartlam, M.; Pei, X.; Rao, Z. Structure of human Spindlin1. *J. Biol. Chem.* **2007**, *282*, 647−656.
(26) Yang, N.; Wang, W.; Wang, Y.; Wang, M.; Zhao, Q.; Rao, Z.; Zhu, B.; Xu, R.-M. Distinct mode of methylated lysine-4 of histone

DOI: 10.1021/acs.jmedchem.9b00522
J. Med. Chem. 2019, 62, 8996−9007

H3 recognition by tandem tudor-like domains of Spindlin1. *Proc. Natl. Acad. Sci. U.S.A.* **2012**, *109*, 17954−17959.
(27) Su, X.; Zhu, G.; Ding, X.; Lee, S. Y.; Dou, Y.; Zhu, B.; Wu, W.; Li, H. Molecular basis underlying histone H3 lysine-arginine methylation pattern readout by Spin/Ssty repeats of Spindlin1. *Genes Dev.* **2014**, *28*, 622−636.
(28) Jiang, F.; Zhao, Q.; Qin, L.; Pang, H.; Pei, X.; Rao, Z. Expression, purification, crystallization and preliminary X-ray analysis of human Spindlin1, an ovarian cancer-related protein. *Protein Pept. Lett.* **2006**, *13*, 203−205.
(29) Franz, H.; Greschik, H.; Willmann, D.; Ozretic, L.; Jilg, C. A.; Wardelmann, E.; Jung, M.; Buettner, R.; Schule, R. The histone code reader SPIN1 controls RET signaling in liposarcoma. *Oncotarget* **2015**, *6*, 4773−4789.
(30) Chen, X.; Wang, Y.-W.; Xing, A.-Y.; Xiang, S.; Shi, D.-B.; Liu, L.; Li, Y.-X.; Gao, P. Suppression of SPIN1-mediated PI3K−Akt pathway by miR-489 increases chemosensitivity in breast cancer. *J. Pathol.* **2016**, *239*, 459−472.
(31) Fang, Z.; Cao, B.; Liao, J.-M.; Deng, J.; Plummer, K. D.; Liao, P.; Liu, T.; Zhang, W.; Zhang, K.; Li, L.; Margolin, D.; Zeng, S. X.; Xiong, J.; Lu, H. SPIN1 promotes tumorigenesis by blocking the uL18 (universal large ribosomal subunit protein 18)-MDM2-p53 pathway in human cancer. *eLife* **2018**, *7*, No. e31275.
(32) Li, Y.; Ma, X.; Wang, Y.; Li, G. miR-489 inhibits proliferation, cell cycle progression and induces apoptosis of glioma cells via targeting SPIN1-mediated PI3K/AKT pathway. *Biomed. Pharmacother.* **2017**, *93*, 435−443.
(33) Chen, X.; Dong, H.; Liu, S.; Yu, L.; Yan, D.; Yao, X.; Sun, W.; Han, D.; Gao, G. Long noncoding RNA MHENCR promotes melanoma progression via regulating miR-425/489-mediated PI3K-Akt pathway. *Am. J. Transl. Res.* **2017**, *9*, 90−102.
(34) Yuan, H.; Zhang, P.; Qin, L.; Chen, L.; Shi, S.; Lu, Y.; Yan, F.; Bai, C.; Nan, X.; Liu, D.; Li, Y.; Yue, W.; Pei, X. Overexpression of Spindlin1 induces cellular senescence, multinucleation and apoptosis. *Gene* **2008**, *410*, 67−74.
(35) Wang, J.-X.; Zeng, Q.; Chen, L.; Du, J.-C.; Yan, X.-L.; Yuan, H.-F.; Zhai, C.; Zhou, J.-N.; Jia, Y.-L.; Yue, W.; Pei, X.-T. Spindline1 promotes cancer cell proliferation through activation of WNT/TCF-4 signaling. *Mol. Cancer Res.* **2012**, *10*, 326−335.
(36) Ciulli, A.; Abell, C. Fragment-based approaches to enzyme inhibition. *Curr. Opin. Biotechnol.* **2007**, *18*, 489−496.
(37) Murray, C. W.; Rees, D. C. The rise of fragment-based drug discovery. *Nat. Chem.* **2009**, *1*, 187−192.
(38) Leeson, P. D.; Springthorpe, B. The influence of drug-like concepts on decision-making in medicinal chemistry. *Nat. Rev. Drug Discovery* **2007**, *6*, 881−890.
(39) Liu, F.; Barsyte-Lovejoy, D.; Allali-Hassani, A.; He, Y.; Herold, J. M.; Chen, X.; Yates, C. M.; Frye, S. V.; Brown, P. J.; Huang, J.; Vedadi, M.; Arrowsmith, C. H.; Jin, J. Optimization of cellular activity of G9a inhibitors 7-aminoalkoxy-quinazolines. *J. Med. Chem.* **2011**, *54*, 6139−6150.
(40) Liu, F.; Barsyte-Lovejoy, D.; Li, F.; Xiong, Y.; Korboukh, V.; Huang, X.-P.; Allali-Hassani, A.; Janzen, W. P.; Roth, B. L.; Frye, S. V.; Arrowsmith, C. H.; Brown, P. J.; Vedadi, M.; Jin, J. Discovery of an in vivo chemical probe of the lysine methyltransferases G9a and GLP. *J. Med. Chem.* **2013**, *56*, 8931−8942.
(41) Vedadi, M.; Barsyte-Lovejoy, D.; Liu, F.; Rival-Gervier, S.; Allali-Hassani, A.; Labrie, V.; Wigle, T. J.; Dimaggio, P. A.; Wasney, G. A.; Siarheyeva, A.; Dong, A.; Tempel, W.; Wang, S.-C.; Chen, X.; Chau, I.; Mangano, T. J.; Huang, X.-p.; Simpson, C. D.; Pattenden, S. G.; Norris, J. L.; Kireev, D. B.; Tripathy, A.; Edwards, A.; Roth, B. L.; Janzen, W. P.; Garcia, B. A.; Petronis, A.; Ellis, J.; Brown, P. J.; Frye, S. V.; Arrowsmith, C. H.; Jin, J. A chemical probe selectively inhibits G9a and GLP methyltransferase activity in cells. *Nat. Chem. Biol.* **2011**, *7*, 566−574.
(42) Sweis, R. F.; Pliushchev, M.; Brown, P. J.; Guo, J.; Li, F.; Maag, D.; Petros, A. M.; Soni, N. B.; Tse, C.; Vedadi, M.; Michaelides, M. R.; Chiang, G. G.; Pappano, W. N. Discovery and Development of Potent and Selective Inhibitors of Histone Methyltransferase G9a. *ACS Med. Chem. Lett.* **2014**, *5*, 205−209.
(43) Oh, B.; Hwang, S. Y.; Solter, D.; Knowles, B. B. Spindlin, a major maternal transcript expressed in the mouse during the transition from oocyte to embryo. *Development* **1997**, *124*, 493−503.
(44) Staub, E.; Mennerich, D.; Rosenthal, A. The Spin/Ssty repeat: a new motif identified in proteins involved in vertebrate development from gamete to embryo. *Genome Biol.* **2001**, *3*, RESEARCH0003.1.
(45) Bae, N.; Gao, M.; Li, X.; Premkumar, T.; Sbardella, G.; Chen, J.; Bedford, M. T. A transcriptional coregulator, SPIN.DOC, attenuates the coactivator activity of Spindlin1. *J. Biol. Chem.* **2017**, *292*, 20808−20817.
(46) Machleidt, T.; Woodroofe, C. C.; Schwinn, M. K.; Méndez, J.; Robers, M. B.; Zimmerman, K.; Otto, P.; Daniels, D. L.; Kirkland, T. A.; Wood, K. V. NanoBRET—a novel BRET platform for the analysis of protein−protein interactions. *ACS Chem. Biol.* **2015**, *10*, 1797−1804.
(47) Green, K. Improved metalation of 2,4,6-tribromoanisole - sythesis of 2-methoxyresorcinol. *J. Org. Chem.* **1991**, *56*, 4325−4326.
(48) Evans, P. Scaling and assessment of data quality. *Acta Crystallogr., Sect. D: Biol. Crystallogr.* **2006**, *62*, 72−82.
(49) Axford, D.; Foadi, J.; Hu, N.-J.; Choudhury, H. G.; Iwata, S.; Beis, K.; Evans, G.; Alguel, Y. Structure determination of an integral membrane protein at room temperature from crystals in situ. *Acta Crystallogr., Sect. D: Biol. Crystallogr.* **2015**, *71*, 1228−1237.
(50) Winn, M. D.; Ballard, C. C.; Cowtan, K. D.; Dodson, E. J.; Emsley, P.; Evans, P. R.; Keegan, R. M.; Krissinel, E. B.; Leslie, A. G. W.; McCoy, A.; McNicholas, S. J.; Murshudov, G. N.; Pannu, N. S.; Potterton, E. A.; Powell, H. R.; Read, R. J.; Vagin, A.; Wilson, K. S. Overview of the CCP4 suite and current developments. *Acta Crystallogr., Sect. D: Biol. Crystallogr.* **2011**, *67*, 235−242.
(51) Winter, G. xia2: an expert system for macromolecular crystallography data reduction. *J. Appl. Crystallogr.* **2010**, *43*, 186−190.
(52) Winter, G.; Waterman, D. G.; Parkhurst, J. M.; Brewster, A. S.; Gildea, R. J.; Gerstel, M.; Fuentes-Montero, L.; Vollmar, M.; Michels-Clark, T.; Young, I. D.; Sauter, N. K.; Evans, G. DIALS: implementation and evaluation of a new integration package. *Acta Crystallogr., Sect. D: Struct. Biol.* **2018**, *74*, 85−97.
(53) Adams, P. D.; Afonine, P. V.; Bunkóczi, G.; Chen, V. B.; Davis, I. W.; Echols, N.; Headd, J. J.; Hung, L.-W.; Kapral, G. J.; Grosse-Kunstleve, R. W.; McCoy, A. J.; Moriarty, N. W.; Oeffner, R.; Read, R. J.; Richardson, D. C.; Richardson, J. S.; Terwilliger, T. C.; Zwart, P. H. PHENIX: a comprehensive Python-based system for macromolecular structure solution. *Acta Crystallogr., Sect. D: Biol. Crystallogr.* **2010**, *66*, 213−221.
(54) Emsley, P.; Lohkamp, B.; Scott, W. G.; Cowtan, K. Features and development of Coot. *Acta Crystallogr., Sect. D: Biol. Crystallogr.* **2010**, *66*, 486−501.
(55) Keller, S.; Vargas, C.; Zhao, H.; Piszczek, G.; Brautigam, C. A.; Schuck, P. High-precision isothermal titration calorimetry with automated peak-shape analysis. *Anal. Chem.* **2012**, *84*, 5066−5073.
(56) Langmead, B.; Trapnell, C.; Pop, M.; Salzberg, S. L. Ultrafast and memory-efficient alignment of short DNA sequences to the human genome. *Genome Biol.* **2009**, *10*, R25.
(57) Zhang, Y.; Liu, T.; Meyer, C. A.; Eeckhoute, J.; Johnson, D. S.; Bernstein, B. E.; Nussbaum, C.; Myers, R. M.; Brown, M.; Li, W.; Liu, X. S. Model-based analysis of ChIP-Seq (MACS). *Genome Biol.* **2008**, *9*, R137.
(58) Scheer, S.; Ackloo, S.; Medina, T.; Schapira, M.; Li, F.; Ward, J.; Lewis, A.; Northrop, J.; Richardson, P.; Kaniskan, H.; Shen, Y.; Liu, J.; Smil, D.; McLeod, D.; Zepeda-Velazquez, C.; Luo, M.; Jin, J.; Barsyte-Lovejoy, D.; Huber, K.; De Carvalho, D.; Vedadi, M.; Zaph, C.; Brown, P.; Arrowsmith, C. A chemical biology toolbox to study protein methyltransferases and epigenetic signaling. *Nat. Commun.* **2019**, *10*, 19.
(59) Kim, Y.; Lee, H.-M.; Xiong, Y.; Sciaky, N.; Hulbert, S. W.; Cao, X.; Everitt, J. I.; Jin, J.; Roth, B. L.; Jiang, Y.-h. Targeting the histone methyltransferase G9a activates imprinted genes and improves

DOI: 10.1021/acs.jmedchem.9b00522
J. Med. Chem. 2019, 62, 8996−9007

survival of a mouse model of Prader-Willi syndrome. *Nat. Med.* **2017**, *23*, 213−222.

DOI: 10.1021/acs.jmedchem.9b00522
J. Med. Chem. 2019, 62, 8996−9007